

# Numerical Simulation on Effects of Laser Fluence on Temporal and Time Integrated LII-Process of Soot Particle

W. Ketren<sup>1,4,\*</sup>, P. Vallikul<sup>2,4</sup>, A. Garo<sup>3</sup>, and G. Grehan<sup>3</sup>

<sup>1</sup> The Joint Graduate School of Energy and Environment, King Mongkut's University of Technology Thonburi, Bangkok, Thailand

<sup>2</sup> Faculty of Engineering, King Mongkut's University of Technology North Bangkok, Thailand

<sup>3</sup> CNRS UMR 6614-CORIA, Université et INSA de Rouen, France

<sup>4</sup> Center for Energy Technology and Environment, Bangkok, Thailand

\*Corresponding Author: wacharakorn@gmail.com Fax: (66)2-470-8626 and Telephone number: (66)9-773-3917

**Abstract:** The primary goal of this study is to analyze the mathematical model of Laser Induced Incandescence (LII) process applied to the measurement of diameter and temperature of a soot particle within flame. To simulate heating and cooling processes of a nanometer size particle, computer codes have been written to calculate the time dependent responses of the particle to laser pulse heating. The results include temperature, diameter, heat losses and LII-signal responses. At low laser fluence heating, the rate of heat losses from the particle is very low in comparison to the rate of heat gain by absorption and LII-signal being sensitive to the temperature of the particle. At high laser fluence heating, the particle sublimates and becomes smaller in diameter. The sublimation cooling is the most important form of heat loss for the particle and is at a comparable rate to the heat gain by absorption. The LII-signal is sensitive to both the temperature and diameter of the particle. Overall (or time integrated) heat transfer and LII-signal over the period of the laser pulse as a function of laser fluence has also been analyzed. The time integration of heat transfer modes over the duration of the laser pulse is represented in the form of an energy balance equation. It has been found that the absorption energy was, at the beginning, stored in the form of internal energy and later lost in the form of sublimation cooling as the laser energy fluence increased. At low laser fluence energy input, the magnitude of the time integrated LII-signal over the laser pulse duration increases with the laser fluence. At high laser fluence energy input, sublimation occurs and the diameter of the particle becomes smaller, undermining the LII-signal. These competing effects, between the internal stored energy gain against the sublimation energy lost, led to the threshold of the time integrated LII-signal at high laser fluence energy inputs. Once the threshold signal is reached, the overall LII-signal becomes less sensitive to the increasing of laser fluence.

**Keywords:** LII-process, soot diameter and temperature, heating and cooling of particle, energy budget.

## 1. Introduction

There is an urgent need to reduce the total emissions from chemical reactions into the atmosphere through improving the efficiency of fuel combustion systems, such as power plants, diesel and spark ignition reciprocating engines, wood stoves, biomass burning and other industrial facilities. This requirement is driven by a fundamental desire to preserve the well-being and health of human being and other living organisms and of the environment. The undesirable exhaust emissions include CO, NO<sub>x</sub>, SO<sub>x</sub>, unburned hydrocarbons, and particulate matter (soot) emitted from both conventional fuel and the bio-fuel. Although there are less concerns on emissions of the CO and SO<sub>x</sub> from the combustion of the bio-fuel such as bio-diesel, one of the major concerns is the formation of soot. Besides the environmental and health concerns, there is also a strong need to control soot and other particulates in the exhaust plume because of their adverse influence on the performance of the power generation systems [1].

Soot consists of small spherical solid particles, aggregated in chains. It participates to small sized respirable aerosols and associated with several serious health effects, including premature death [2]. People with asthma, cardiovascular or lung disease, as well as children and elderly people, are considered to be the most sensitive to the effects of fine particulate matter. Soot is also responsible for environmental effects such as corrosion, soiling, damage to vegetation, and it reduces visibility [3].

To limit soot emissions, a suitable means for reliably measuring various soot-related parameters [3] must be developed. Laser-induced incandescence (LII) technique is a recent measurement method that has been adapted for expeditious measurements to characterize the soot within combustion flames [4]. There are two kinds of LII-measurements. The first is based on the record and treatment of time averaged 2D image. The images are formed

by the thermal radiation emitted by soot particles after their heating by a pulse laser sheet. The LII signals are averaged and form the 2D LII-image, assumed to be proportional to the soot volume fraction [4].

The second kind of LII method consists in analyzing the time dependent LII-signal emitted by soot particles: the soot particles are first heated by a laser pulse [5] of few nanoseconds duration, then cooled by different modes of heat transfer. The numerical simulation of a soot particle behavior during the heating then cooling periods is compared with the measurement data. The diameter and temperature of soot within the measuring volume are obtained when simulated and experimental LII signals are in good agreement. In the simulation, the LII signals depend strongly on the models chosen for the heat transfer.

This paper will focus on the development of a numerical simulation of the time dependent heat transfers during the LII-process. The effects of laser fluence on the heat and mass transfer from the soot particle computed in order to analyze the time evolution of the temperature and the size of the soot particle. The integration versus time of each separate term of the balance energy equation allows the analysis of the sensitivity of the time integrated LII-signal to the laser fluence, respectively.

## 2. Modeling the Laser-Induced Incandescence (LII) Process of Soot

The physical interpretation of the LII-process is illustrated in Fig. 1. Fig. 1a shows a schematic diagram of a particle being heated by different Gaussian laser intensity profiles. The diagram illustrates the fact that, given high enough laser energy a spherical solid particle may sublime then its diameter reduces.

Fig. 1b shows the different heat transfer modes occurring at any instantaneous time during the heat transfer processes. The net heat transfer results in the rate of change of internal energy

of the particle. In this section, the numerical modeling of heat and mass transfers during the LII-process will be given in detail. The model used in this work is based on the first LII model, established by Melton [5]. It mainly consists in the energy and the continuity equations.

**2.1 The governing equations of the LII process**

Assuming that the particle temperature is uniform during the whole LII process, the mathematical model describing the rate of change of internal energy of the soot is the following:

$$\frac{dU_{Internal}}{dt} = \dot{Q}_{Absorption} - \dot{Q}_{Conduction} - \dot{Q}_{Sublimation} - \dot{Q}_{Radiation} \tag{1}$$

The soot particle heat gain corresponds to the absorption of the laser beam energy and the heat losses are generated by the conduction, radiation and sublimation phenomena.

Since sublimation results in the particle mass loss, a supplementary equation governing the change of the particle diameter is needed for a closure problem. The particle is assumed to keep its spherical shape all along its evolution. During the sublimation process, the continuity equation of mass flux indicates that the rate of mass loss from the particle is equal to the mass leaving the surface of the particle in the form of mass flux of carbon vapor or:

$$-\frac{dM}{dt} = \rho_v U_v A, \tag{2}$$

$\rho_v U_v$  is the carbon vapor mass flux leaving the surface and  $A$  is the particle surface area.

**2.2 Numerical modeling of diameter**

Equation (2) stands for the carbon mass sublimated from the particle surface continually. Changing the rate of mass loss into the form of diameter, we have:

$$\frac{dM}{dt} = \frac{d(\rho_s \frac{1}{6} \pi D^3)}{dt} = \rho_s \frac{\pi}{2} D^2 \frac{dD}{dt} \tag{3}$$

$$-\rho_s \frac{1}{2} \frac{dD}{dt} = \rho_v U_v \tag{3}$$

The average vapor velocity,  $U_v$ , of the sublimation carbon vapor is given by the molecular speed of an ideal gas [5] as

$$U_v = \sqrt{\frac{R_m T}{2W_v}} \tag{4}$$

The gas density,  $\rho_v$ , that appears in the equation (3) can be determined from the ideal gas equation of state given the values of mass accommodation factor,  $\alpha_M$ , the molecular weight,  $W_v$ , of the carbon vapor and the gas constant  $R_m$ , i.e.:

$$\rho_v = \frac{\alpha_M W_v P}{R_p T} \tag{5}$$

The carbon vapor at the surface is in thermal equilibrium with the solid carbon at the particle surface then,  $T=T_v$ . The vapor pressure  $P_v$ , introduced in equation (5), is related to the vapor temperature at the surface through the Clausius-Clapeyron equation:

$$P_v = P^* \exp\left(\frac{\Delta H_{sub}(T - T^*)}{RTT^*}\right) \tag{6}$$

where  $P^*$  and  $T^*$  are reference pressure and temperature at 1 bar and 3915 K respectively. The latent heat for sublimation,  $\Delta H_{sub}$ , used is  $7.78 \times 10^{-5}$  J/mol. Substituting Equations (4) to (6) into the equation (2) and rearranging, we get the time derivative of the particle diameter:

$$\frac{dD}{dt} = -\frac{2}{\rho_s} \left(\frac{R_m T}{2W_v}\right)^{\frac{1}{2}} \left(\frac{\alpha_M W_v}{R_p T}\right) P^* \exp\left(\frac{\Delta H_{sub}(T - T^*)}{RTT^*}\right) \tag{7}$$

The rate of diameter change shown above in Equation (7) is a function of temperature, whose parameters are assumed to be constants. Note that  $R$ ,  $R_m$  and  $R_p$  are all referred to gas constants but in different systems of unit which values are listed in the Nomenclature table.

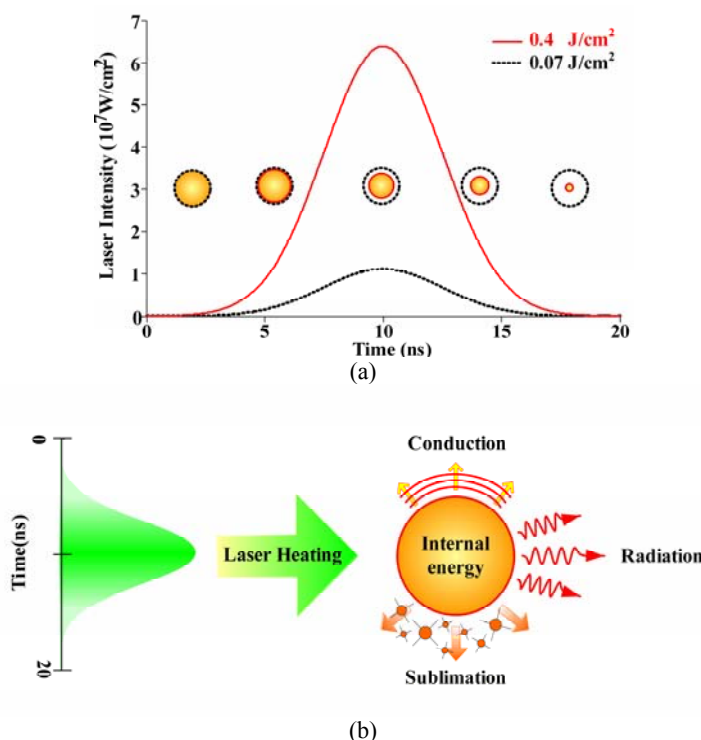


**Figure 1.** Schematic diagram for a soot particle being heated by a laser pulse at nanosecond time duration a) Diameter changes and b) Different rate of heat transfer modes during the laser heating process.

### 2.3 Modeling the rates of energy transfer

The internal energy can be represented by the particle temperature and the rate of change of the internal energy term can be replaced by:

$$\frac{dU_{\text{Internal}}}{dt} = m_s C_s \frac{dT}{dt} = \rho_s \frac{\pi}{6} D^3 C_s \frac{dT}{dt} \quad (8)$$

where  $C_s$  and  $\rho_s$  are the density and the specific heat of the solid carbon whose values are assumed constant and equal to 1.90 J/g·K and 2.26 g/cm<sup>3</sup> respectively [6].

In this simulation, the temporal laser intensity profile,  $q(t)$ , is a Gaussian profile, defined by:

$$q(t) = F \frac{1}{\sigma\sqrt{2\pi}} \exp\left(-\frac{(t-t_{\text{center}})^2}{2\sigma^2}\right) \quad (9)$$

where  $F$ , the laser fluence, is a model parameter in this simulation. By definition, it is equal to the time integration of the laser power over the pulse period. The values of  $\sigma$  and  $t_{\text{center}}$  used in the normalized Gaussian function are 2.5 and 10 ns respectively.

The rate of laser energy absorption per second can be calculated from:

$$\dot{Q}_{\text{Absorption}} = \frac{\pi^2 D^3 E(m)}{\lambda_1} q(t) \quad (10)$$

where  $E(m)$  is the complex index of refraction of the particle,  $m = n_m - ik_m$ ,  $n_m$  and  $k_m$  represent the real and the imaginary parts of refractive index respectively,  $\lambda_1$  being the laser excitation wavelength.

There are many published works that mention the spectral dependence of  $E(m)$  having been measured by a combination of light extinction, with correction for light scattering, and comparison with gravimetric determination of soot concentration [7]. However, in this work, however, it is assumed that  $E(m) = 0.23$  at the laser excitation wavelength of 532 nm [6]. The energy absorption rate then becomes:

$$\dot{Q}_{\text{Absorption}} = \frac{\pi^2 D^3}{\lambda_1} E(m) \left[ F \frac{1}{\sigma\sqrt{2\pi}} \exp\left(-\frac{(t-t_{\text{center}})^2}{2\sigma^2}\right) \right] \quad (11)$$

The heat conduction loss is proportional to the difference between the particle surface temperature and the surrounding gas temperature. It is assumed that the initial surface temperature of the particle is equal to the gas temperature ( $T(t=0)=T_0$ ). The heat conduction at the boundary of the particle is equal to the convection in transition regime according to the approach of McCoy and Cha [8], i.e.:

$$\dot{Q}_{\text{Conduction}} = \frac{2\kappa_a \pi D^2}{(D+GL)} (T-T_0) \quad (12)$$

where  $\kappa_a$  is the thermal conductivity of the surrounding gases,  $L$  is the mean free path, and  $T_0$  is the temperature of ambient gases. The values of  $\kappa_a$  and  $L$  are constant and equal to  $1 \times 10^{-3}$  W/cm·K and  $2.355 \times 10^{-8} T_0$  cm respectively. The heat transfer factor  $G$  is given by the following equation:

$$G = \frac{8f}{\alpha_T(\gamma+1)} \quad (13)$$

where  $\alpha_T$  is the thermal accommodation coefficient and  $\gamma$  is the heat-capacity ratio of air whose values are 0.3 and 1.3 respectively. The Eucken correction as the equation was also proposed by Michelsen [6] to the thermal conductivity is given by:

$$f = \frac{9\gamma-5}{4} \quad (14)$$

The particle is assumed to be blackbody and the radiation loss follows Stefan-Boltzmann radiative transfer equation:

$$\dot{Q}_{\text{radiation}} = \pi D^2 \sigma_{SB} (T^4 - T_0^4) \quad (15)$$

where  $\sigma_{SB}$  is the Stefan-Boltzmann constant and equal to  $5.6704 \times 10^{-12}$  W/cm<sup>2</sup>K<sup>4</sup>.

The sublimation loss results in the change of the particle mass and reducing its diameter. A rigorous model of sublimation has been introduced by Michelsen [6], it takes into account of the effects of different carbon cluster decay C1, C2... C10. But this is far more complicated, and sometimes being not necessarily justified to choose all types of the carbon decay. The soot decomposes mainly in C3 carbon cluster as can be seen by Smallwood et al. [9].

In this study, the classical Melton [5] sublimation model is used. The rate of sublimation cooling through the mass loss, is expressed as

$$\dot{Q}_{\text{Sublimation}} = -\frac{1}{W_v} \frac{dM}{dt} \Delta H_{\text{sub}} = -\frac{\Delta H_{\text{sub}} \pi}{W_v} \rho_s D^2 \frac{dD}{dt} \quad (16)$$

The derivative in the right hand side of equation (16) can be written in temperature and diameter variables, as given by equation (7), and hence:

$$\dot{Q}_{\text{Sublimation}} = \frac{\Delta H_{\text{sub}}}{W_v} \pi D^2 P^* \exp\left(\frac{\Delta H_{\text{sub}}(T-T^*)}{RTT^*}\right) \left(\frac{\alpha_M}{R_p}\right) \left(\frac{R_m W_v}{2}\right)^{1/2} \frac{1}{\sqrt{T}} \quad (17)$$

By substitution of Equations (8), (11), (12), (13), (15) and (17) into Equation (1), we obtain the equation describing the changed rate of particle temperature in response to laser heating:

$$\frac{dT}{dt} = \frac{6\pi}{\rho_s C_s \lambda} E(m) F \frac{1}{\sigma\sqrt{2\pi}} \exp\left(-\frac{(t-t_{\text{center}})^2}{2\sigma^2}\right) - \frac{2\kappa_a}{\rho_s C_s D(D+GL)} (T-T_0) - \frac{6\Delta H_{\text{sub}}}{\rho_s C_s D W_v} P^* \exp\left(\frac{\Delta H_{\text{sub}}(T-T^*)}{RTT^*}\right) \left(\frac{\alpha_M}{R_p}\right) \left(\frac{R_m W_v}{2}\right)^{1/2} \frac{1}{\sqrt{T}} - \frac{6}{\rho_s C_s D} \sigma_{SB} (T^4 - T_0^4) \quad (18)$$

Equations (7) and (18) form a system of equations whose solution is the time evolution of the temperature and the diameter of the particle under the LII-process. The temperature and diameter obtained are used to determine the LII-signal emitted from the particle.

### 2.4 The LII-signal

The LII-signal is the spectral emitted power at wavelength,  $\lambda$ , from the Planck function, integrated over solid angle and the particle surface area, emitted from a soot particle, hence:

$$S_{\lambda_s} = \varepsilon_{\lambda_s} D^2 \frac{2\pi^2 hc^2}{\lambda_s^5} \left[ \exp\left(\frac{hc}{k_B \lambda_s T}\right) - 1 \right]^{-1} \quad (19)$$

where  $h$  is the Planck constant,  $c$  is the speed of light,  $k_B$  is the Boltzmann constant, and  $\lambda_s$  is the emission wavelength which are  $6.626 \times 10^{-34}$  J·s,  $2.998 \times 10^{10}$  cm/s,  $1.381 \times 10^{-23}$  J/K and 500 nm respectively. The spectral emissivity,  $\varepsilon_{\lambda_s}$ , is given as [6]:

$$\varepsilon_{\lambda_s} = \frac{4\pi DE(m)}{\lambda_s} \quad (20)$$

where  $E(m)$  has already been defined in Equation (11). After replacing the emissivity,  $\varepsilon_{\lambda_s}$ , of equation (19) by the value given by Equation (20) we then have:

$$S_{\lambda_s} = \frac{8\pi^3 D^3 hc^2 E(m)}{\lambda_s^6} \left[ \exp\left(\frac{hc}{k_B \lambda_s T}\right) - 1 \right]^{-1} \quad (21)$$

Note that the LII-signal defined in equation (21), is a time dependent signal and vary with the particle temperature and diameter.

### 3. Results and Discussion

To study the heat transfer and LII-signal responses, several intensity profiles of the Gaussian laser pulses have been simulated corresponding to different energy fluences: 0.05, 0.07, 0.2, 0.4 and 0.7 J/cm<sup>2</sup> have been simulated (see Fig. 2) to serve as the heat source of a fictitious soot particle. The first two values of the laser fluences correspond to low laser fluence then to low heating since the sublimation of the particle can be ignored. Effects of laser fluence on heat losses and on LII-response are delineated in this section; both in terms of time dependent and time integrated functions. Calculations were performed using a laser excitation wavelength of 532 nm, a primary particle of 30 nm of diameter, at an enviroing gas temperature of 1800 K (equal to the temperature of the particle) and ambient pressure of 1 bar. The signal emitted by the particle is calculated at an emission wavelength of 500 nm.

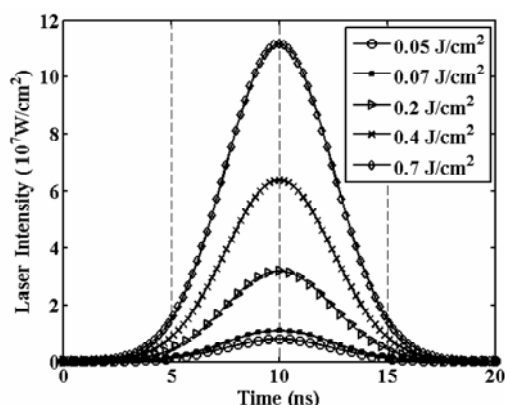


Figure 2. Time dependent laser intensity profile at different laser fluences.

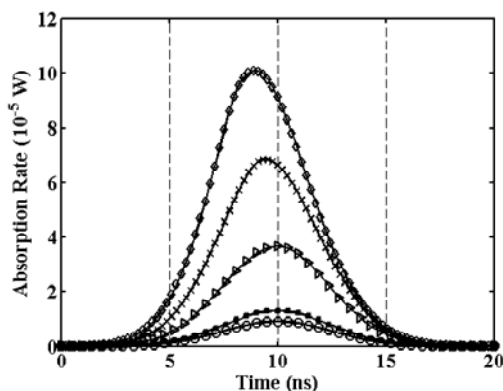


Figure 3. Time dependent absorption rate at different laser fluences.

#### 3.1 Temporal response of heat losses and LII-signals

The absorption energy profiles at different laser fluence are shown in Fig. 3. The absorption profiles at low fluence follow the laser pulse of Gaussian profile; meaning that most of the laser absorbed power is transformed in the form of internal energy. At high laser fluence, the absorption profiles deviate from the Gaussian profile particularly after the maximum: there are significant heat losses from the particle.

By comparing the values of about 10<sup>-5</sup> W the maximum rate of heat gain during absorption to the maximum rate of heat losses due to sublimation conduction and radiation being at the orders of 10<sup>-5</sup>, 10<sup>-8</sup> and 10<sup>-8</sup> W respectively (see Fig. 4, 5 and 6), it can be concluded that only sublimation heat losses are in comparable rate to the absorption heat gain rates. The conduction and radiation losses occur at much lower rates.

Fig. 4 shows that sublimation cooling occurs at high laser fluences: 0.2, 0.4 and 0.7 J/cm<sup>2</sup>. When heating at higher rate, the sublimation occurs earlier and lasts shortly after the end of laser pulse. After that the cooling processes controlled by the radiation and conduction losses at lower rates.

Figs 5 and 6 show similar trends for conduction and radiation cooling processes: the heat losses increase with time but once sublimation takes place the cooling rates decrease. This is due to the reduction of heat transfer surface area of the particle.

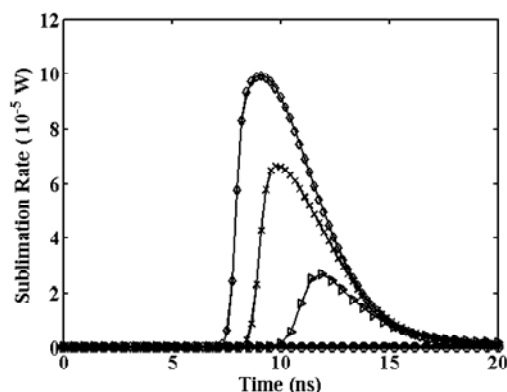


Figure 4. Time dependent sublimation rate at different laser fluences.

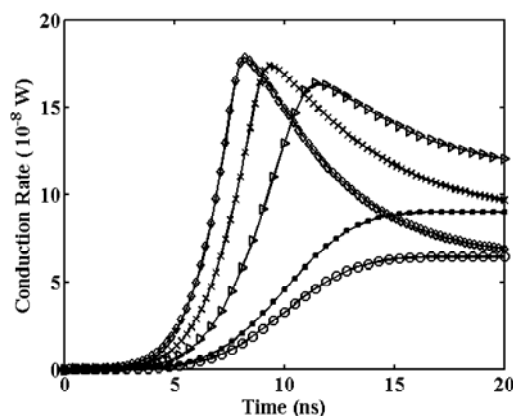


Figure 5. Time dependent conduction rate at different laser fluences.

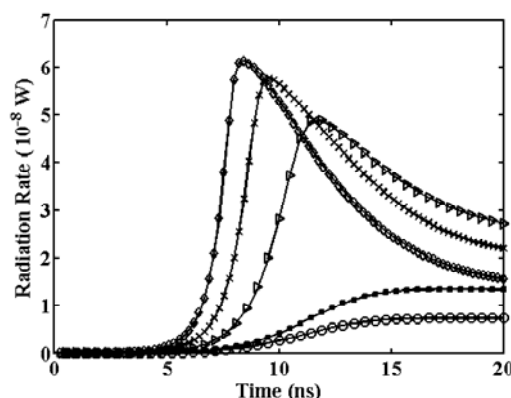


Figure 6. Time dependent radiation rate at different laser fluences.

In Fig. 7 the particle diameter changes negligibly when using low laser fluence heating, but at high laser fluence the particle sublimates and its diameter decreases.

Temporal response of the particle temperature to the laser heating pulse is shown in Fig. 8. While heating at different laser fluences, the temperature rises at different rates; logically, at the highest laser fluences which are used, corresponds with the highest the rate of temperature. The maximum value of temperature which is reached, depends on sublimation process mainly.

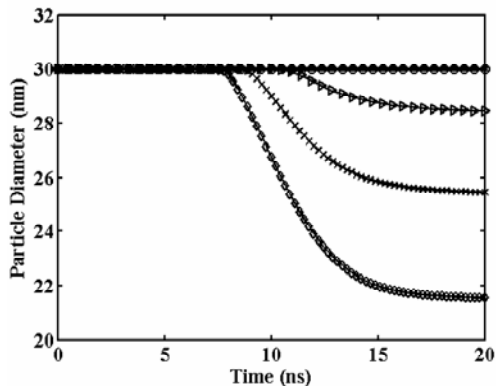


Figure 7. Time dependent particle diameter at different laser fluences.

The time dependent LII-signals are shown in Fig. 9. It is clear that during the particle's laser pulse, the LII-signal changes with both particle temperature and diameter. The two parameters consecutively control the LII-signals at different evolution time at high laser fluence heating: before the particle's sublimation (constant diameter heating) the LII-signal varies with the temperature thereafter (constant temperature heating) it varies with the particle diameter.

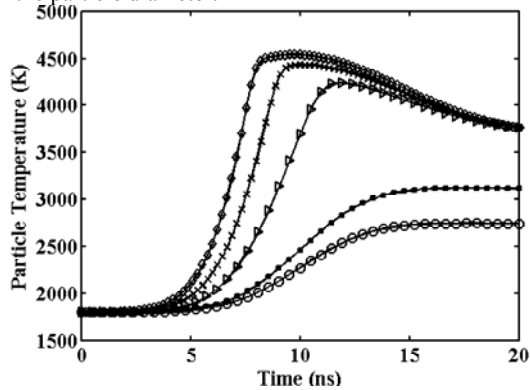


Figure 8. Time dependent particle temperature at different laser fluences.

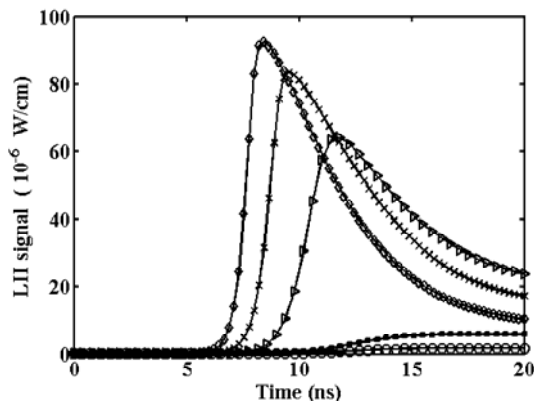


Figure 9. Time dependent LII-signal at different laser fluences.

### 3.2 Energy budget and time integrated LII-signal

To have information on total energy gains and losses for each mode of heat transfer on the soot particle related to the laser energy absorbed, the time integration of each energy transfer mode over the laser pulse period is advanced resulting in an energy budget representation. Since the time integration is limited to a finite duration then the rate of internal energy change exists and the energy remains within the particle as stored energy. It has to be added up to the other mode of heat losses in order to balance with the energy absorbed by the particle.

Fig. 10 shows the time integrated energy ratios during a laser pulse (20 ns) period against laser fluence. It can be seen

that most of the absorbed energy is stored in the form of internal energy. The energy losses due to sublimation, radiation and conduction are negligible at these low levels of laser fluence ( $<0.1 \text{ J/cm}^2$ ). Once the laser fluence is large enough, sublimation occurs and the absorbed energy shares one part to the internal energy and the other part to the sublimation loss.

If the integration time scale is beyond that of a laser pulse period then the slower responses of conduction and radiation heat losses can be accommodated into the energy budget. It can be seen from Fig. 11 that the radiation contributes within less than 10% whereas the conduction contributes more than 30% of the absorbed energy at low laser fluence heating. Although the radiation is to the fourth power of temperature, the particle is of a nano-size, limiting the total amount of radiation area. Whereupon the occurrence of sublimation at higher laser fluence, the conduction and radiation losses ratios become lower which combination of the two being negligibly low in comparison to the sublimation loss. The size of the particle is also smaller when the particle sublimates. Therefore at these high laser fluences heating, most of the particle's absorbed energy is lost in the sublimation process.

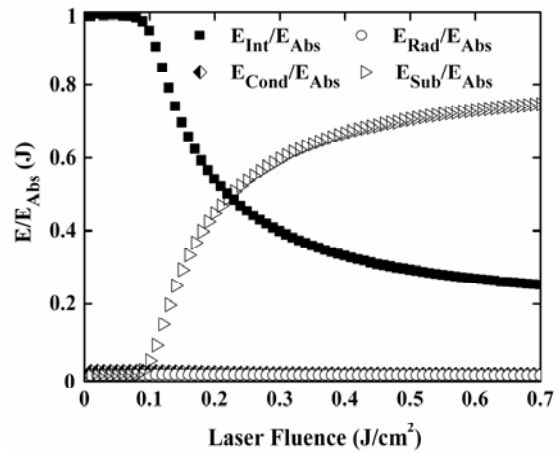


Figure 10. Time integrated energy ratios against laser fluence (integrate over 20 ns).

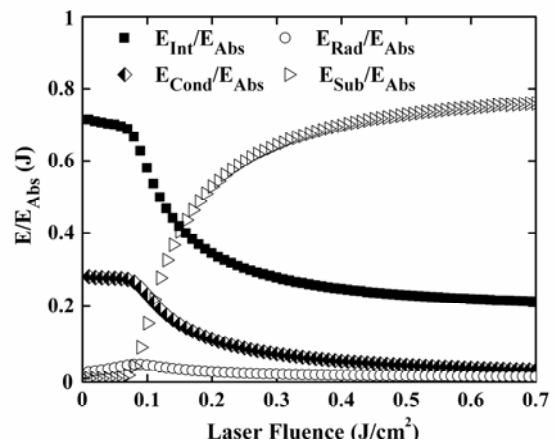


Figure 11. Time integrated energy ratios against laser fluence (integrate over 300 ns).

The integration, over 20 ns laser pulse period, of LII-signal versus laser fluences is plotted in Fig. 12. The LII-signal increases as the laser fluence increases until the laser fluence arrives at a certain value where the LII-signal is maximum. The maximum point is due to the fact that the temperature of the particle is limited by the sublimation temperature of the particle. Once the sublimation temperature arrives, the diameter of the particle reduces due to mass transfer in the sublimation process. At that temperature, the LII-signal becomes less sensitive to the

temperature but more to the diameter changes; the smaller the diameter, the less the LII-signal is. These similar trends can be found when comparing the results from the integration over other time scales. Once the threshold level of LII-signals have been reached the signals then become lower and later are less sensitive to the high level of laser fluence.

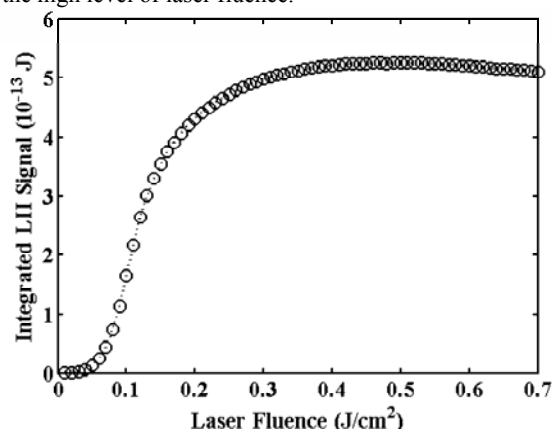


Figure 12. Time integrated LII-signal against laser fluence.

#### 4. Conclusion

The LII-process of a soot particle was simulated using heat transfer model based on Melton model and model parameters with input laser Gaussian profile, particle size of 30 nm-diameter, and ambient conditions. The effects of laser fluence on the heat transfer modes and the strength at LII-signal of the soot particle, both the temporal and time integrated responses, were also simulated.

During the laser pulse, it was found that the conduction and radiation heat losses were negligibly low in comparison to the absorption rate. At low laser fluence, most of the absorbed rate is transformed into the rate of internal energy stored within the carbon particle. While at high laser fluence, the absorption power transforms into the sublimation cooling rate. After the laser pulse, the conduction heat becomes more significant than other modes of heat losses from the particle. Before the particle reaches its peak temperature, the temporal LII-signal is controlled by the rate of change of temperature. After the temperature peak, the LII-signal is controlled by the rate of change in the particle diameter to the existence of the sublimation process. Otherwise, the signal depends only on the rate of change of temperature.

Time integration of rate of heat transfer is demonstrated in the energy budget representation. For short time scale integration, within a single laser pulse interval, the absorbed energy transforms mostly into internal energy. With increased laser fluence, part of the absorbed energy is also lost in the form of sublimation cooling. For longer time scale integration, the energy budget accommodates the slower modes of heat transfer: conduction and radiation. Most energy is lost due to conduction at low energy fluence heating, but to the sublimation at high energy fluence.

Time integration of the LII-signal increases with laser energy fluence in response to the increasing rate of change of the temperature. However, the signal becomes less sensitive to the laser fluence at higher levels. This is because the particle sublimates at high laser fluence and the LII-signal is undermined.

Although the effects of laser fluence on the temporal and time integrated LII-process of a soot particle were simulated, the simulation is limited to the fully constrained model, with some model parameters being assumed as constant with only a single size of the initial diameter of the soot particle. The simulation study on the effects of the laser fluence on the LII-process by relaxing all or some of the limitations has yet to be further explored.

#### Nomenclature

$c$	The speed of light in a medium; $2.998 \times 10^{10}$ (cm/s)
$C_s$	The specific heat of the solid particle; $2.26$ (g/cm <sup>3</sup> )
$D$	Primary particle diameter; initial primary particle diameter is $30 \times 10^{-7}$ (cm), <i>i.e.</i> 30 (nm)
$E(m)$	Dimensionless refractive-index function.
$F$	Laser fluence (J/cm <sup>2</sup> ); $0.05$ J/cm <sup>2</sup> for low laser fluence and $0.7$ J/cm <sup>2</sup> for high laser fluence.
$f$	Dimensionless Eucken correction to the thermal conductivity
$G$	Dimensionless geometry- dependent heat-transfer factor
$h$	The Planck's constant; $6.6263 \times 10^{-34}$ (J-s)
$\Delta H_{sub}$	Average enthalpy of formation of sublimed carbon; $7.78 \times 10^{-5}$ (J/mol)
$k_B$	Boltzmann constant; $1.3813 \times 10^{-23}$ (J/K)
$L$	Mean free path; $2.355 \times 10^{-8} T_0$ (cm) for Melton model
$M$	Particle mass (g)
$P_0$	Ambient pressure (1 bar = 0.98692 atm)
$P_v$	Average partial pressure of sublimed carbon species (bar).
$P^*$	Reference pressure used in Clausius-Clapeyron equation.
$q(t)$	The temporal laser of intensity profile
$\dot{Q}_{Absorption}$	Rate of energy gained by laser absorption (Watt)
$\dot{Q}_{Conduction}$	Rate of energy lost by conduction to surrounding gases (Watt)
$\dot{Q}_{Radiation}$	Rate of energy lost by radiative emission (Watt)
$\dot{Q}_{sublimation}$	Rate of energy lost by sublimation (Watt)
$R$	Universal gas constant; $8.3145$ (J/mol-K)
$R_m$	Universal gas constant in effective mass unit ; $8.3145 \times 10^7$ (g-cm <sup>2</sup> /mol-K-s)
$R_p$	Universal gas constant in effective pressure unit ; $83.145$ (bar-cm <sup>3</sup> /mol-K)
$S_{\lambda_s}$	Calculated LII Signal (W/cm) at 500 nm over the entire particle surface time (s)
$t$	Time (s)
$T$	Particle temperature (K)
$T^*$	Reference temperature used in Clausius-Clapeyron equation; $3915$ (K)
$U_{Internal}$	Internal energy of particle (J)
$W_V$	Average molecular weight of sublimed carbon particle (J/mol)
<b>Greek Alphabet</b>	
$\alpha_M$	Species-independent mass accommodation coefficient of Vaporized carbon clusters; 1
$\alpha_T$	Thermal accommodation coefficient of ambient gases with the Surface; 0.3
$\gamma$	Heat capacity ratio for the gas surrounding the particles; 1.3
$\epsilon_\lambda$	Emissivity at wavelength, $\lambda_s$ .
$\kappa_a$	Thermal conductivity of ambient gas; $1 \times 10^{-3}$ (W/cm-K)
$\lambda_l$	Laser wavelength; $532 \times 10^{-7}$ (cm), <i>i.e.</i> 532 (nm)
$\lambda_s$	Emission wavelength for signal calculation ; $500 \times 10^{-7}$ (cm), <i>i.e.</i> 500 (nm)
$\pi$	Pi constant, 3.14
$\rho_s$	Density of solid carbon; $2.26$ (g/cm <sup>3</sup> )
$\sigma_{SB}$	Stefan-Boltzmann constant; $5.6704 \times 10^{-12}$ W/cm <sup>2</sup> -K <sup>4</sup> )

### References

- [1] Knothe G, Dunn RO, Bagby MO, *Biodiesel: The Use of Vegetable Oils and Their Derivatives as Alternative Diesel Fuels*, Oil Chemical Research, National Center for Agricultural Utilization Research, Agricultural Research Service, U.S. Department of Agriculture, Peoria, IL 61604.
- [2] Harrison RM, Shi JP, Jones MR, Continuous Measurements of Aerosol Physical Properties in the Urban Atmosphere, *Atmospheric Environment* 33/7 (1999) 1037-1047.
- [3] John PA, Makkee NM, Moulijn JA, Diesel particulate emission control, *Fuel Processing Technology* 47 (1996) 1-69.
- [4] Ni T, Pinson JA, Gupta S, Santoro RJ, Two-dimensional Imaging of Soot Volume Fraction by the Use of Laser- Induced Incandescence, *Applied Optics* 34 (1995) 7083- 7091.
- [5] Melton LA, Soot diagnostics based on laser heating, *Applied Optic* 23/13 (1984) 2201-2206.
- [6] Michelsen HA, Understanding and predicting the temporal response of laser-induced incandescence from carbonaceous particles, *Journal of Chemical Physics* 118 (2003) 7012-7045.
- [7] Krishnan SS, Lin KC, Faeth GM, Optical Properties in the Visible of Overfire Soot in Large Buoyant Turbulent Diffusion Flames, *Journal of Heat Transfer* 122/3 (2000) 517-524.
- [8] McCoy BJ, Cha CY, Transport phenomena in the rarefied gas transition regime, *Chemical Engineering Science* 29/2 (1974) 381-388.
- [9] Snelling DR, Smallwood GJ, Liu F, Gülder ÖL, Bachalo WD, A calibration-independent laser-induced incandescence technique for soot measurement by detecting absolute light intensity, *Applied Optics* 44 (2005) 6773-6785.